

We are IntechOpen, the world's leading publisher of Open Access books Built by scientists, for scientists

6,900

Open access books available

186,000

International authors and editors

200M

Downloads

Our authors are among the

154

Countries delivered to

TOP 1%

most cited scientists

12.2%

Contributors from top 500 universities



WEB OF SCIENCE™

Selection of our books indexed in the Book Citation Index
in Web of Science™ Core Collection (BKCI)

Interested in publishing with us?
Contact book.department@intechopen.com

Numbers displayed above are based on latest data collected.
For more information visit www.intechopen.com



Chapter

The Modeling, Design, Fabrication, and Application of Biosensor Based on Electric Cell-Substrate Impedance Sensing (ECIS) Technique in Environmental Monitoring

Xudong Zhang, William Wang and Sunghoon Jang

Abstract

In this research, the modeling, design, fabrication, and application of ECIS sensors in environmental monitoring are studied. The ECIS sensors are able to qualify the water toxicity through measuring the cell impedance. A novel mathematical model is proposed to analyze the distribution of electric potential and current of ECIS. This mathematical model is validated by experimental data and can be used to optimize the dimension of ECIS electrodes in order to satisfy environmental monitors. The detection sensitivity of ECIS sensors is analyzed by the mathematical model and experimental data. The simulated and experimental results show that ECIS sensors with smaller radius of working electrodes yield higher impedance values, which improves signal-to-noise ratio, which is more suitable in measuring the cell morphology change influenced by environments. Several ECIS sensors are used to detect the toxicant including, phenol, ammonia, nicotine, and aldicarb, and the decreasing cell impedance indicates the toxic effect. The gradient of measured impedance qualitatively indicates the concentration of toxicants in water.

Keywords: ECIS, biosensor, sensitivity, model, electrodes, design, fabrication

1. Introduction

A large number of the world's population live in areas with high risks of environment. Industrialization and usage of nonbiodegradable and non-eco-friendly material are harmful to the environment. Rapid urbanization, increasing population, and extensive agriculture all are threats to the Earth's supply of fresh water. Clean and reliable drinking water can be guaranteed by periodic and extensive testing. Effectively and efficiently environmental monitoring approaches are

necessary. ECIS sensing is one of the techniques among them. The ECIS is becoming an increasingly popular technique, which is able to analyze cell behaviors by measuring the impedance profile spectroscopy [1, 2]. The measured cell impedance provides information about cell morphology and electric properties, including intercellular junction conditions, numbers and densities, attachment, migration, proliferation, invasion, barrier function, membrane capacitance, and cytoplasm conductivity [1–6]. A common ECIS sensor is composed of a working electrode and a counter electrode. Some types of ECIS sensors have a third electrode, the reference electrode, which is used to provide the reference voltage for electrochemical measurements. The traditional ECIS sensors are fabricated on rigid substrate that limits the application in some of dynamically moving environments. Zhang et al. [7, 8] have fabricated the ECIS sensors on stretchable polymer. Such sensors are able to simulate in vitro the dynamic environment of organisms, such as pulsation, bending, and stretching, which enables investigations on cell behavior that undergoes mechanical stimuli in biological tissue [9–12].

The cells, attaching and spreading on the ECIS sensors, behave like an insulating medium after seeding. The insulating medium restricts the ion movement between the electrodes [13, 14]. As a result, the measured impedance increases gradually as more cells attach onto the surface. When the cells form a monolayer on the electrodes, the impedance becomes stabilized. The impedance may fluctuate slightly due to cell attachment migration, deformation, and detachment [9, 15–18]. Some chemical, biological, or physical stimuli on measured cells will influence the impedance response due to the changes in cell monolayer caused by cell-cell interactions, cell-substrate interactions, or changing cell electrical properties [2, 9]. Recently, the application of ECIS sensors has been extended to cell-based assays and toxicity study [18].

The ECIS sensors have different configurations including working electrode dimensions, counter electrode dimensions, and distance between electrodes. However, the relationship between the electrode configuration and detection sensitivity has not been further studied. A study on detection sensitivity of ECIS sensors is meaningful for sensor design, fabrication, and applications.

Detection sensitivity is critical in the applications of ECIS sensors, which depends on sensor configuration, such as electrode dimension and the distance between the electrodes [19]. Wang et al. studied the detection sensitivity of ECIS sensors only with interdigital electrodes [20]. Several mathematical models have been introduced to analyze the relationship between measured cell impedance and cell morphology and behaviors [1, 2, 10, 21–28]. In those models, cell membrane and cell cytoplasm were assumed to be capacitors and resistors, respectively, and cell impedance was calculated as a combination of the capacitors and resistors [24–28]. However, the current may switch from one path to another or creating a hybrid path in reality, which was considered by some models [1, 2, 10, 14]. Nevertheless, these models assumed that the current flows radially between the substratum and the ventral surface of the cell, and the electric potential is constant inside the cell. However, the electric potential cannot be assumed to be constant inside the cell if the current flows through the entirety of the cell. This assumption is invalidated by Ohm's law.

In this study, the influence of ECIS sensor configuration on detection sensitivity and the analysis of paths of current flow of ECIS have been carried out for improving the detection sensitivity, design, and application of ECIS sensors. The ECIS sensors are optimized for water toxicity testing. Several ECIS sensors are used to perform the toxicity testing in detecting the toxic effects from phenol, ammonia, nicotine, and aldicarb, and the impedance response successfully indicate the toxic effect. The gradient of measured impedance qualitatively is related to the concentration of toxicants.

2. The mathematical model of electric cell-substrate impedance sensing (ECIS)

In order to monitor the environments effectively, systematically analyzing the relationship between the electric properties of measured subjects and output of ECIS sensors are needed. In this section, a model related to electric field distribution of ECIS sensing, which can be used in quantifying the ECIS sensor measurements, is created with a partial differential equation. The model of ECIS is established in cylindrical coordinates (r, θ, z) as shown in **Figure 1** and simplified into polar coordinates (r, z) due to its axisymmetric property.

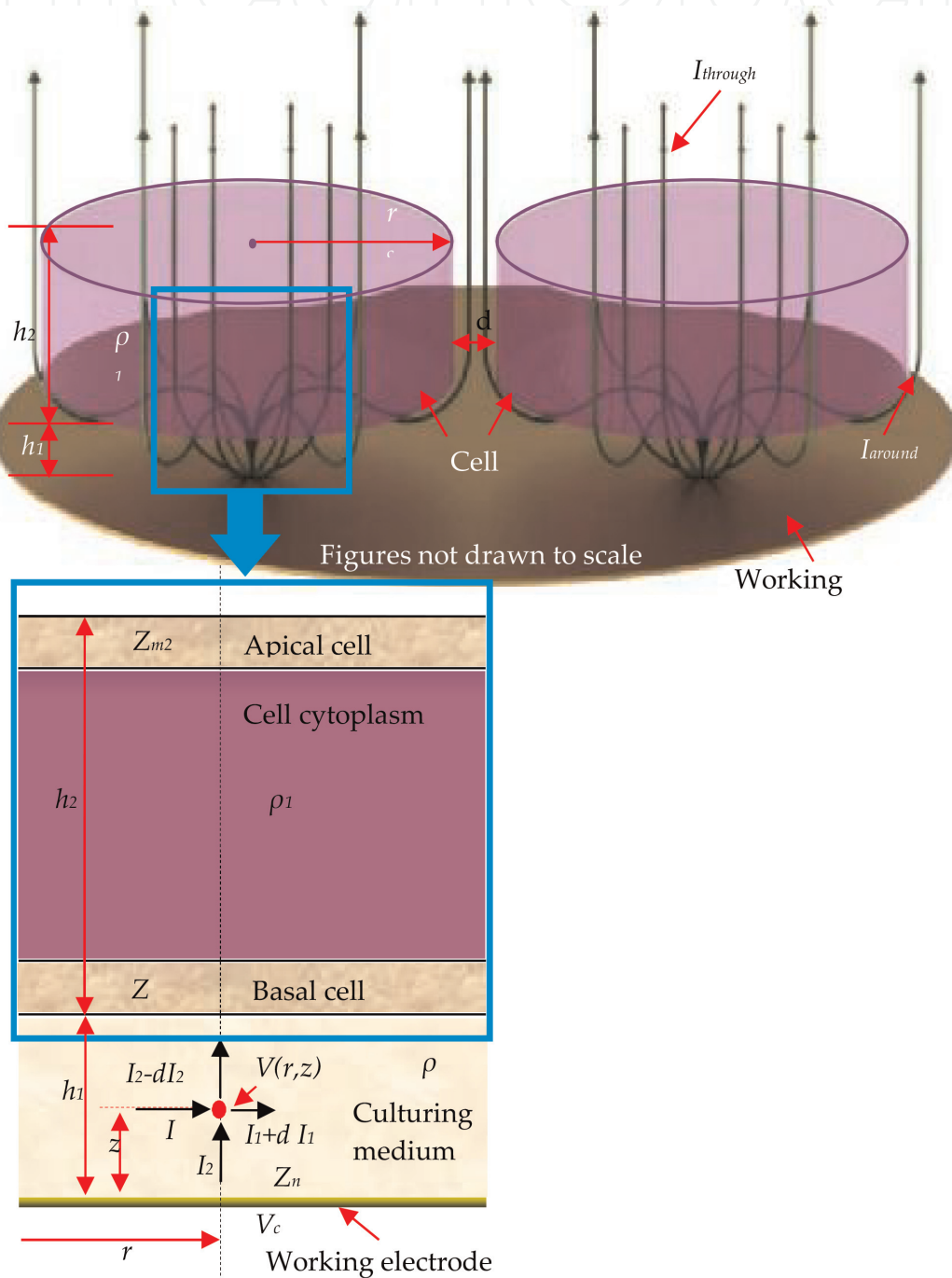


Figure 1. Illustration of cell impedance sensing on a working electrode. The electric potential at the coordinate (r, z) is $V(r, z)$. ρ and ρ_1 are the resistivity of the cell culture medium and cytoplasm respectively. Z_{m1} , Z_{m2} and Z_n are the specific impedance of the basal, apical cell membrane, and electrode-electrolyte interface respectively (in Ωm). h_1 is the average distance between the ventral surface of cell and electrode-electrolyte interface. h_2 is the average thickness of the cell. d is the average horizontal distance between adhesive cells. V_c is the electrical potential on the working electrode.

The governing equation of electric field distribution of ECIS sensing (as shown in Eq. (1)) can be obtained from the differential form of Ohm's law between electric potential and current (as shown in Eq. (2)), Kirchhoff's circuit law at a point of interest (r, z) (as shown in Eq. (3)), and the gradient of electric potential (as shown in Eq. (4)). The solution of the governing equation is shown in Eq. (5), which is the same as the solution in Giaever et al. ECIS model when the variable z is held as constant [1, 2, 23, 29]. The detailed information about the mode can be referred to in [19]. These three coefficients A , D , and c are calculated as $A = -2.3$, $D = 3.3$, and $c = 4749.83$ by using the parameters listed in [19, 30–36].

$$\frac{2\pi z}{-\rho} \left(\frac{\partial V}{\partial r} + r \frac{\partial^2 V}{\partial r^2} \right) - \frac{2\pi r}{-\rho} \left(\frac{\partial V}{\partial z} \right) = 0 \quad (1)$$

$$\rho \left(\frac{I_1}{2\pi r z} e_r + \frac{I_2}{\pi r^2} e_z \right) = E \quad (2)$$

$$I_1 + I_2 = I_1 + dI_1 + I_2 - dI_2 \quad (3)$$

$$\frac{\partial V}{\partial r} e_r + \frac{\partial V}{\partial z} e_z = -E \quad (4)$$

$$V(r, z) = AI_0(2cr)e^{2c^2z^2} + D \quad (5)$$

where ρ is the resistivity of the cell culture medium (electrolyte); I_1 and I_2 are the current flowing through the point (r, z) in r and z directions, respectively; e_r and e_z are the unit vectors of the r and z directions; E is the electric field at any point (r, z) ; V is the electric potential at the point (r, z) ; and dI_1 and dI_2 are the infinitesimally small currents of I_1 and I_2 . dI_1 and dI_2 have the same sign; $I_0(2cr)$ is the modified Bessel function of the first kind; A , D , and c are the coefficients of solution $V(r, z)$.

2.1 The calculated impedance of a single cell

In this model, the impedance of a single cell ($Z_{single\ cell}$) is able to be calculated by dividing the electric potential difference between the apical $V(r_c, h_1)$ and ventral surfaces of a single cell $V(r_c, h_1 + h_2)$ by the total current flowing through and around the cell, as shown in Eq. (6).

$$\begin{aligned} Z_{single\ cell} &= \frac{V(r_c, h_1) - V(r_c, h_1 + h_2)}{I_2 + I_j} \\ &= \frac{\left(\rho_1 h_2 \sqrt{\sigma^2 + (2\pi f \epsilon \epsilon_0)^2} + 2t \right) (2I_0 + 2cr_c I_1)}{2\pi \left[r_c^2 I_0 \sqrt{\sigma^2 + (2\pi f \epsilon \epsilon_0)^2} + \frac{r_c d}{\rho \alpha h_2} \left(\rho_1 h_2 \sqrt{\sigma^2 + (2\pi f \epsilon \epsilon_0)^2} + 2t \right) (2I_0 + 2cr_c I_1) \right]} \end{aligned} \quad (6)$$

where I_2 is the current flowing through a single cell, I_j is the current flowing through the intercellular junction gap; h_1 is the average distance between the ventral surface of cell and electrode-electrolyte interface; h_2 is the average thickness of the cell layer; r_c is the average radius of a single cell; f is the measurement frequency; ρ_1 is the resistivity of cell cytoplasm; ϵ is the relative permittivity of the cell membrane; ϵ_0 is the vacuum permittivity, which is 8.85×10^{-12} F/m; and t and σ are the thickness and conductivity of the cell membrane, respectively.

2.2 The calculated impedance of a cell monolayer

The impedance of a cell monolayer (Z) is calculated as the sum of the impedance on current path, including the impedance from working electrode $Z_{working}$, counter electrode $Z_{counter}$, and cell culture medium R_s , as shown in Eq. (7).

$$Z = Z_{working} + Z_{counter} + R_s = \left(\frac{1}{S_1} + \frac{1}{S_2} \right) \left[Z_n + \frac{S(Z_{single\ cell} + Z_{cell_sub})}{n} \right] + R_s \quad (7)$$

where Z_n is the specific impedance of the electrode-medium interface (unit Ωm^2), which can be calculated according to the parameters referred to [19, 37–41]; S_1 and S_2 are the surface areas of the working and counter electrodes, respectively; S is the total surface area of the ECIS sensor, which contains the working electrode, counter electrode, and nonelectrode area; n is the number of cells seeded on the ECIS sensor; R_s is the impedance of the culture medium, which can be calculated according to the parameters referred to [19, 42–47]; Z_{cell_sub} is the impedance of the culture medium between the electrode-electrolyte interface and ventral surface of cell, which can be calculated by dividing the electric potential difference between the edge and center of a single cell by the total current flowing through and around the cell [19].

3. The design of ECIS sensors for environmental monitoring

The design of ECIS sensors includes the dimensions of working electrodes and counter electrodes, and the distance between them is critical in environmental monitoring because those designing parameters will influence the detection sensitivity of ECIS sensors.

3.1 The design guideline of electrode dimensions of ECIS sensors

The radius of working electrode (R_i) and the distance between the edges of the sensing electrodes (d_{io}) can be optimized by using the mathematical model with the parameters related to cell morphology and electric properties and surrounding culture medium.

3.1.1 The relationship between the radius of working electrode (R_i) and cell impedance

During impedance measurements, ions move through the cell monolayer between the working and counter electrodes which follow many paths. The counter electrodes must have adequate sensing area in order to provide adequate circuit connection. The larger R_i working electrode provides more current paths, which decreases the corresponding impedance. Higher impedance values can improve the data quality of the measured impedance by increasing signal-to-noise ratio, which is useful particularly for sensing small changes in cell behavior. However, the working electrode should not be too small in order to measure adequate number of cells and to guarantee sufficient cell-to-cell contact area.

In this study, the ECIS sensors with R_i from 100 to 400 μm were fabricated to analyze the relationship between R_i and measured cell impedance. **Figure 2** illustrates the cell morphology on those sensors. The simulated cell impedance by using R_i within the same range was also obtained from the mathematical model. The experimental and simulated impedance of cell were shown in **Figure 3**. The

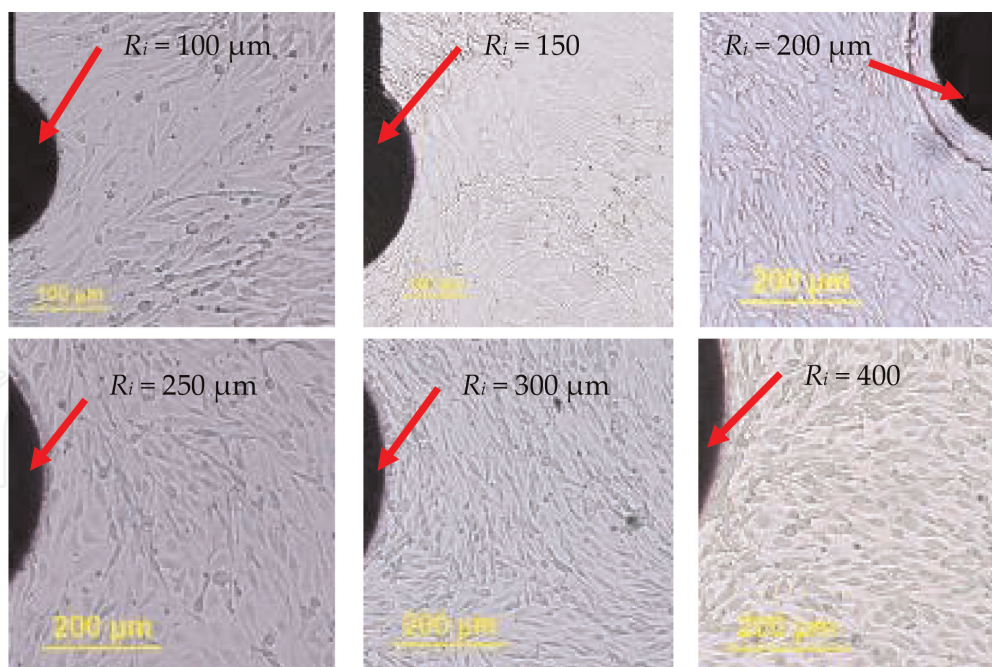


Figure 2. BAEC monolayer on ECIS sensors with different R_i ($d_{i0} = 3.5$ mm).

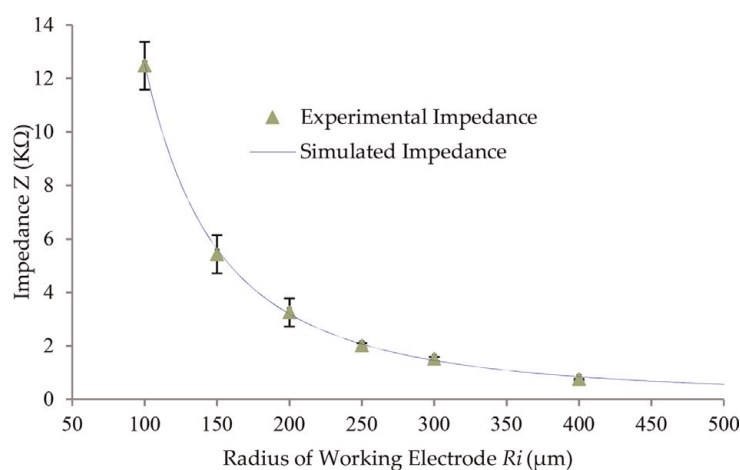


Figure 3. Relationships between R_i and experimental impedance, and between R_i and simulated impedance at 8000 Hz ($n = 4 \sim 6$, $d_{i0} = 3.5$ mm).

simulated impedance curve matches the experimental data closely with maximum difference 13.29%, which is acceptable when considering the fluctuation of measured impedance. The consistency of the simulated impedance with the experimental impedance validates this model's ability to optimize the R_i according to the range of measured cell number and expected output impedance level during sensor designing.

3.1.2 The relationship between the distance between the edges of the sensing electrodes (d_{i0}) and cell impedance

The distance between the edges of the sensing electrodes (d_{i0}) is another factor that should be considered in designing ECIS sensors. **Figure 4** shows the experimental impedance and the simulated impedance with different d_{i0} . The average experimental impedance slightly changed from 12.50 to 12.52 K Ω , when d_{i0} changed from 1000 to 3500 μm . The simulated impedance was calculated by using Eq. (7).

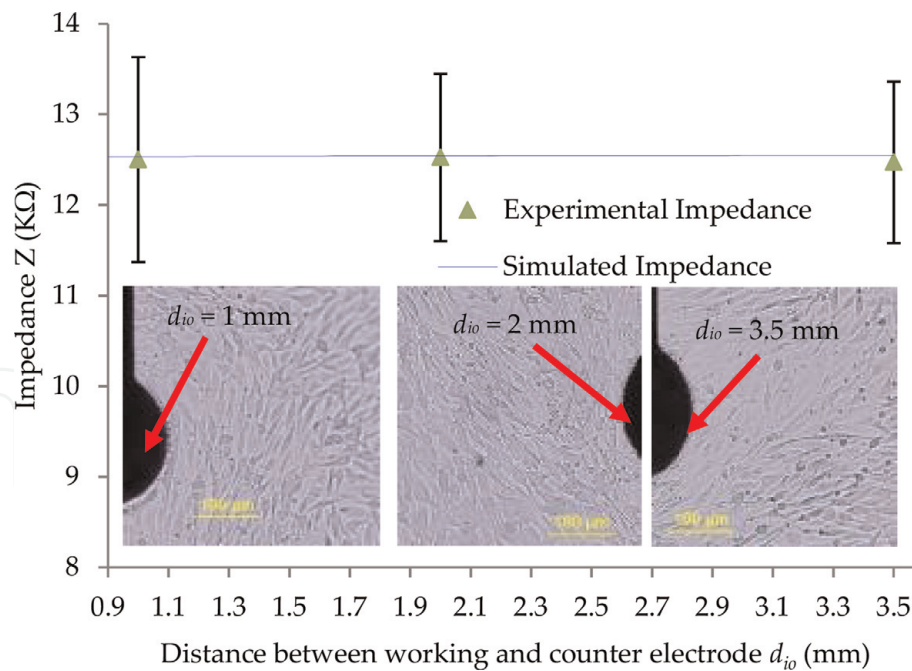


Figure 4. Relationships between d_{io} and experimental impedance, and between d_{io} and simulated impedance, measured at 8000 Hz ($n = 6 \sim 7$, $R_i = 100 \mu\text{m}$). The three images show the cell morphology of BAECs on the ECIS sensors with d_{io} of 1 mm, 2 mm, and 3.5 mm, respectively.

d_{io} only slightly influences the simulated impedance because the natural logarithm of the quotient of $(R_i + d_{io})$ and R_i makes the influence of d_{io} on simulated impedance more slightly in Eq. (7). The simulated impedance is consistent with the experimental data with maximum difference 0.63%, which validates the model. The experimental and simulated impedance indicates that d_{io} in the range of 1000–3500 μm has only a little influence on the impedance because d_{io} influenced the impedance of medium, which is only a small portion of measured impedance. Thus, d_{io} cannot dramatically influence the measured impedance. However, d_{io} should be large enough to avoid the current bypassing the cell monolayer between sensing electrodes.

3.2 The influence of electrode dimensions on the detection sensitivity of ECIS

Detection sensitivity reflects the fineness of impedance response to the changes of cell behavior in cell-based assay environmental monitoring. The detection sensitivity of ECIS sensors is influenced by R_i . According to the previous experimental results, ECIS sensors with R_i larger than 200 μm do not respond sensitively and quickly on cell morphology changes. So, ECIS sensors with R_i of 100 and 150 μm were fabricated to study the influence of R_i on the detection sensitivity. Cell densities, 90,000, 100,000, and 110,000 cells/ cm^2 , were used to study the relationship between cell density and impedance. **Figure 5** shows the impedance shifts versus the cell density changes with R_i of 100 and 150 μm . **Figure 6** shows the corresponding cell morphology on different ECIS sensors. When the cell density changes are 10,000 cells/ cm^2 (from 90,000 to 100,000 cells/ cm^2), the impedance increased 597 and 350 Ω for the sensors with R_i of 100 and 150 μm , respectively. When the cell density changes are 20,000 cells/ cm^2 (from 90,000 to 110,000 cells/ cm^2), the impedance increased 1336 and 880 Ω for the sensors with R_i of 100 and 150 μm , respectively. The experimental results indicate that the sensors with larger R_i illustrate less impedance changes with the same amount of cell density changes. Therefore, the sensors with smaller R_i are able to detect more

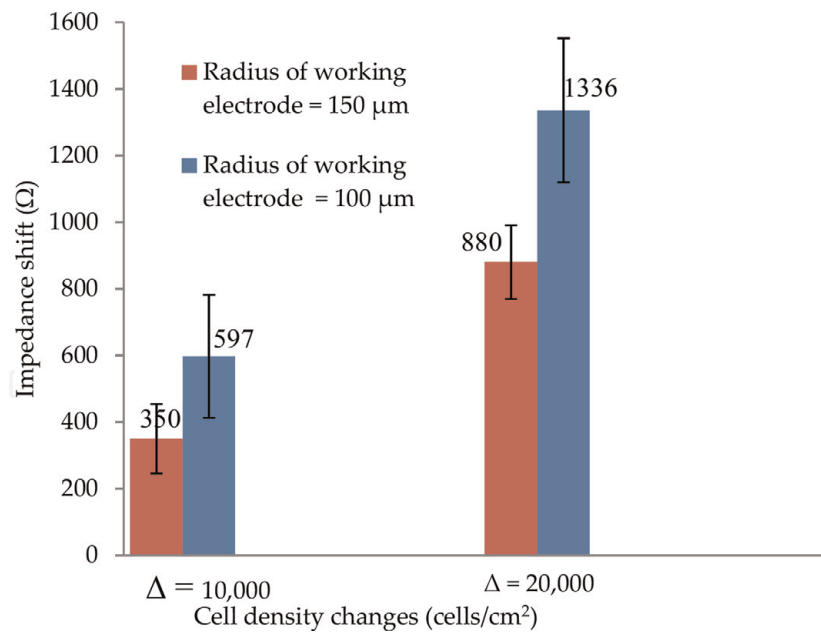


Figure 5. Impedance shifts to cell density changes with sensors' R_i of 100 μm and 150 μm ($n = 3$). The cell density change from 90,000 cells/ cm^2 to 100,000 or 110,000 cells/ cm^2 .

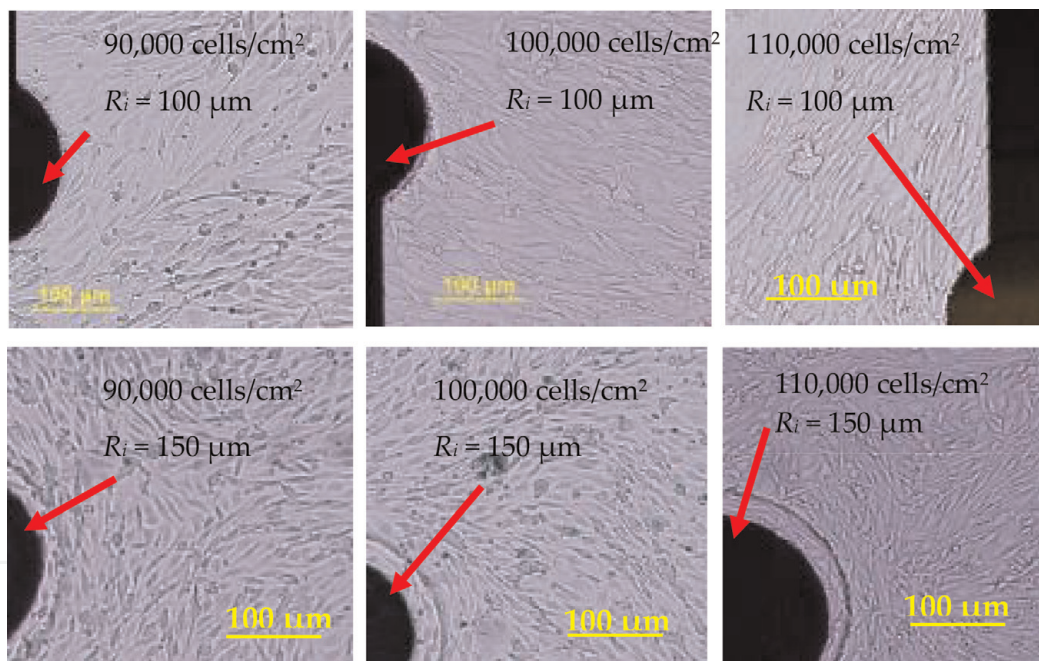


Figure 6. Cell morphology with 90,000, 100,000, and 110,000 cells/ cm^2 cell densities on ECIS sensors ($R_i = 100 \mu\text{m}$ and $R_i = 150 \mu\text{m}$).

sensitive changes in cell density. Therefore, ECIS sensors with smaller dimension working electrodes illustrate better detection sensitivity on changes in cell density. Another benefit is that smaller R_i requires fewer cells in cell-based assays.

Based on the analysis above, the ECIS sensors with R_i of 100–125 μm and d_{io} of 3.5 mm are preferred in environmental monitoring because R_i of 100–125 μm will allow the ECIS sensors to be sensitive to sense the cell morphology changes due to environment influence and own good anti-interference ability. The area of counter electrodes should be as large as possible to guarantee sufficient contact area between electrode and cells. d_{io} of 3.5 mm is enough to avoid the current bypassing the cell layer in ECIS measurements.

4. Fabrication of ECIS sensor arrays

The fabrication of ECIS sensors can follow different photolithography techniques. The substrates are usually nonconductive materials, includes glass, printed circuit board (PCB) [1–4, 19, 23], and polymer including polydimethylsiloxane (PDMS) [9] and polycarbonate [1–3, 18, 19]. The ECIS arrays were fabricated on glass by thin film deposition and lift-off photolithography technique, as shown in **Figure 7**. Initially, the photoresist AZ5214E (MicroChemicals, Somerville, NJ) was coated on glass slides with spinning coater at 2000 rpm. After baking on hotplate at 110°C for 50 seconds, the coated photoresist was exposure to ultraviolet (UV) light. Then, a reversal bake is carried out at 120°C for 2 minutes. Finally, UV light with intensity larger than 200 mJ/cm² was exposure on the photoresist pattern. The electrode pattern was created after immersing the slides with photoresist in the AZ 100 Remover (MicroChemicals, Somerville, NJ). The remover is able to dissolve the photoresist without the first exposure (image reverse). A 20-nm-thick chromium (Cr) followed by a 150-nm-thick gold (Au) was coated on the substrate to form the sensor's electrodes by thermal evaporation. The sensing electrodes were formed after the lift-off process. Then, the photoresist SU-8 (MicroChem, Westborough, MA) was used to cover the substrate except the sensing areas. The sensor arrays were treated with 95% sulfuric acid at 60°C for 15 seconds [48] followed by washing with deionized water (DI) and then treated with 8% (3-aminopropyl) triethoxysilane (APTES) at 50°C for 2 hours to improve the surface biofunctionality. Finally, cell culture wells (Lab-Tek 8-well culture wares) were glued onto the sensor array. **Figure 8** shows the fabricated ECIS sensor array and its configuration. R_i is the radius of the working electrode, R_{co} is the outer radius of the

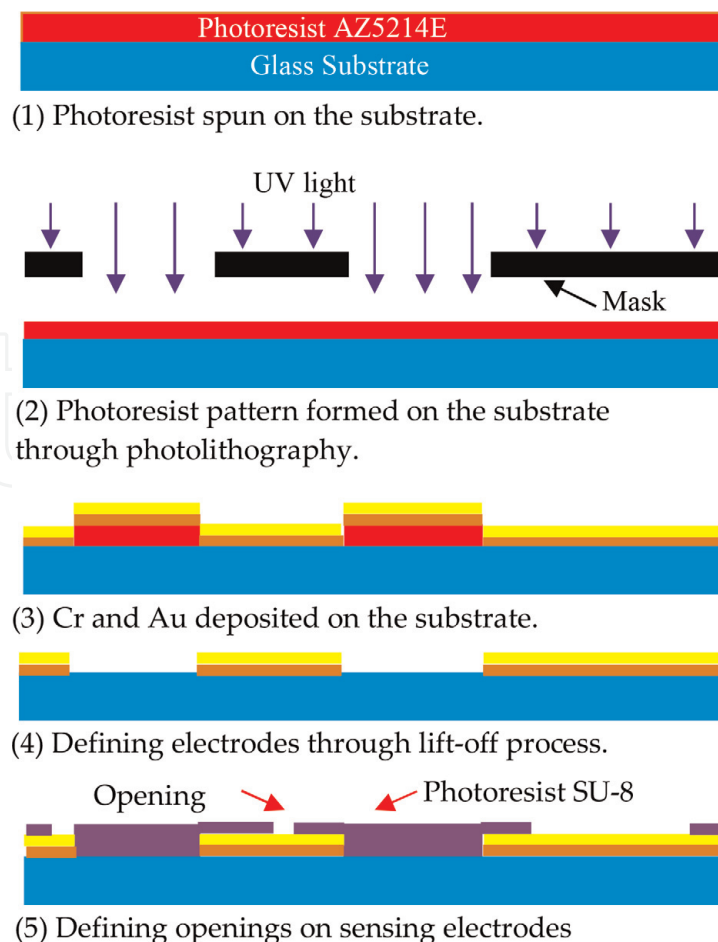


Figure 7.
Illustration of ECIS sensor fabrication.

(Figure not drawn to scale)

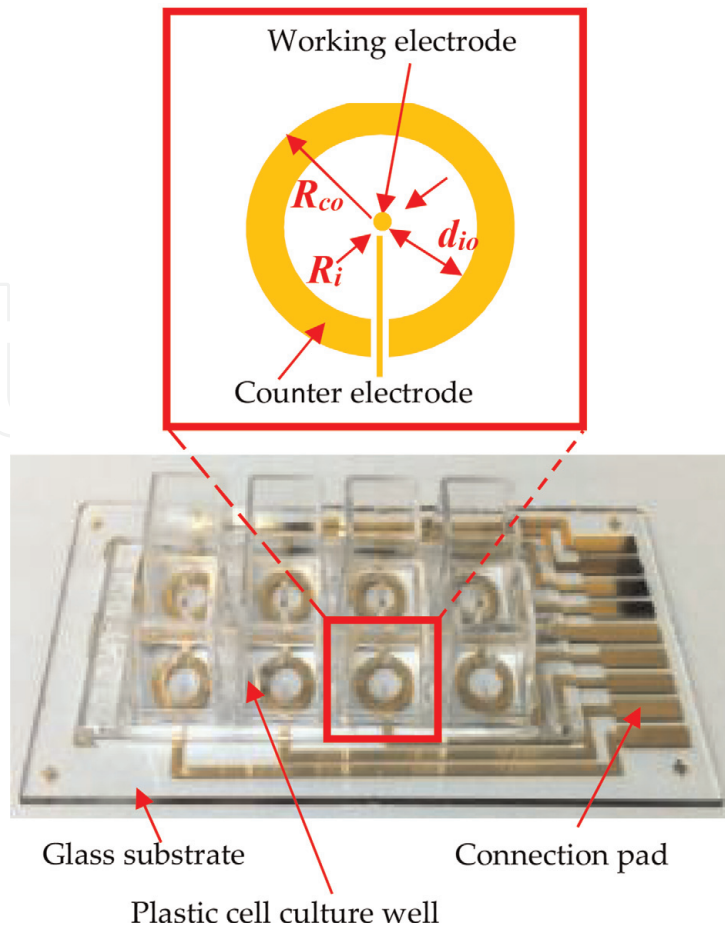


Figure 8.
The array of eight ECIS sensors.

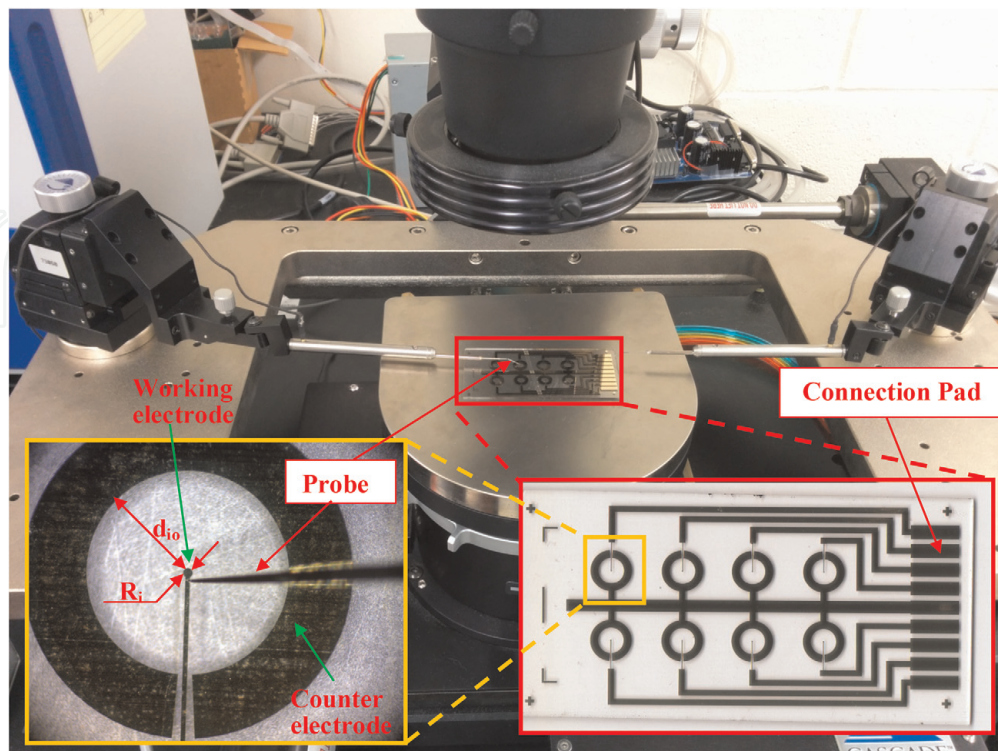


Figure 9.
Distribution of equipotential lines in the space between the ventral cell surface and electrode-electrolyte interface layer. The axisymmetric axis of the cell locates at $x = 0$ (red dashed line).

counter electrode, d_{io} is the distance between the edges of the electrodes, and S_1 and S_2 are the areas of the working and counter electrodes, respectively.

The inherent impedance of the Au/Cr electrodes of fabricated ECIS sensors is measured by microwave probe station (Cascade Microtech Inc., Beaverton, OR) and impedance analyzer (Agilent 4294) as shown in **Figure 9**. The maximum inherent impedance was 19Ω at 8000 Hz, which is much lower than the measured cellular impedance of thousands of ohms. Thus, the inherent impedance of the sensor can be neglected.

5. The application of ECIS sensors in environmental monitoring

5.1 Cell culture and preparation

Bovine aortic endothelial cells (BAECs, VEC Technologies, Rensselaer, NY) were used in this study. The BAECs were cultured in minimum essential medium (MEM, GIBCO, Grand Island, NY) with 10% fetal bovine serum (FBS, GIBCO, Grand Island NY) under standard mammalian cell culturing conditions (37°C and 5% CO_2). Confluent BAEC were trypsinized to detach the cells from the cell culture flasks to prepare the cell suspension. Then, the cell suspension was centrifuged on the bottom of centrifuge tube followed by aspirating off the upper supernatant. Finally, certain amount of cell culture medium was added into centrifuge tube to prepare specific concentration of the cell suspension.

5.2 Toxicant preparation

This study investigated the toxicant detection by using the ECIS sensors. The toxicants used in this study are phenol (RICCA, Arlington, TX), ammonia (Acros Organics, Fair Lawn, NJ), nicotine (Fisher Scientific, Hanover Park, IL), and aldicarb (SPEX CertiPrep, Metuchen, NJ). All the toxicants were diluted with Dulbecco's phosphate-buffered saline (DPBS, Mediatech, Inc., Manassas, VA). The osmolarity of diluted toxicant solution was considered to be in the suitable range for cell culture because the small volume of toxicants added into DPBS will not change the concentration of essential ingredients of DPBS dramatically.

5.3 Experimental system setup

Impedance analyzer Agilent 4294 and ECIS measurement system (Applied Biophysics, Troy, NY) was used to measure the cell impedance. The AC signal applied to the cells was monitored by using Tektronix oscilloscope DPO2014B. Two MAXIM DG408 Multiplexers, controlled by an NI USB-6008 multifunction data acquisition card, were used as a 16-channel multiplexer between the impedance analyzer and the sensor arrays. The NI USB-6008 and Agilent 4294 were controlled by LabVIEW programs to perform the data acquisition shown as **Figure 10**. The ECIS sensor arrays, covered with BAECs on the sensing electrodes, were kept in an incubator with 37°C and 5% CO_2 during the impedance measurement.

5.4 Optimization of cell seeding density and measurement frequency

The cell seeding density and measurement frequency are need to be optimized to obtain reasonable measurement results. BAECs were seeded with different cell densities of 150,000, 125,000, and 100,000 cells/ cm^2 on ECIS sensor. The impedance values were recorded and normalized in the initial 46 hours after seeding onto

the ECIS sensor array, as shown in **Figure 11**. The morphology of cells with seeding density $125,000 \text{ cells/cm}^2$ at different time points was also shown in **Figure 11**. The cells gradually spread on the surface of ECIS sensors after seeding and eventually form a monolayer with stable impedance. The cell impedance gradually increased in the initial 8–20 hours, which indicates the initial formation of a loose monolayer and stable up to the end of the impedance measurements. The cell morphology was

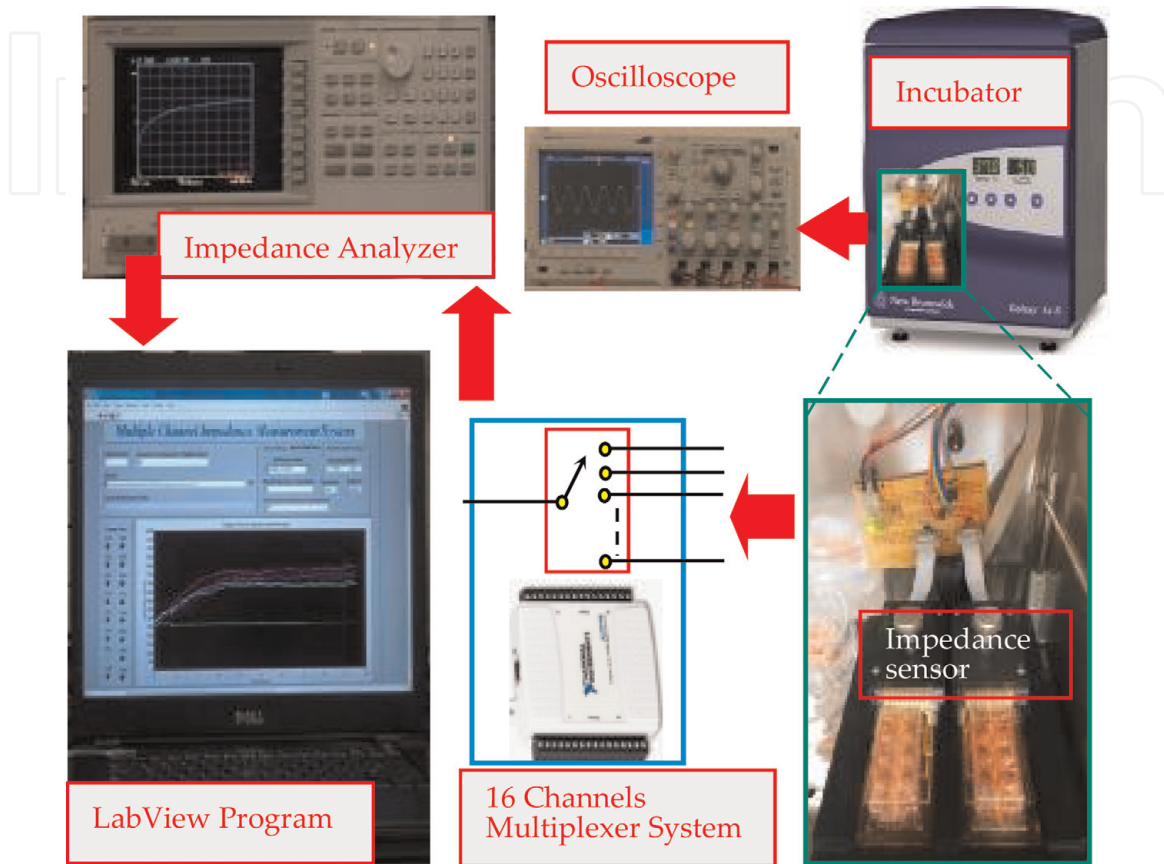


Figure 10. Experimental setup of cell impedance measurement.

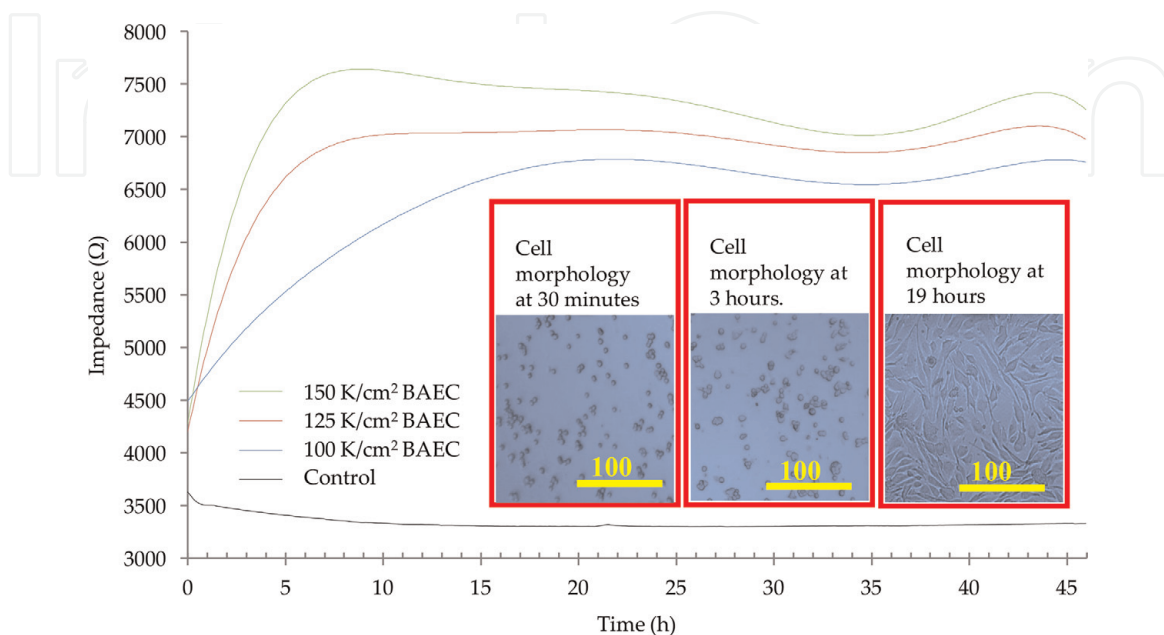


Figure 11. Impedance response of BAECs measured by an ECIS sensor array at 8000 Hz and the image of cell morphology.

checked under microscope frequently. The corresponding impedance readings were used to represent the impedance of the cell monolayer for cell-based assays. In **Figure 11**, the impedance of cell monolayer with higher seeding densities increases more rapidly than cells with lower seeding densities because higher seeding densities allow the cells to have tighter and stronger intercellular junctions and the corresponding ion insulating abilities are better. The impedance of cells with the highest seeding density, 150,000 cells/cm², decreased after initial formation (around 8 hours) of cell monolayer due to the cell movement on the surface of ECIS sensors. Also, the impedance of cells with 150,000 cells/cm² seeding density is not stable as those with 125,000 and 100,000 cells/cm² seeding densities. The cells with a seeding density of 100,000 cells/cm² need 20 hours to be confluent and have low impedance compared with those with higher seeding densities. Hence, the cell seeding density, 125,000 cells/cm², was chosen as the preferred seeding density in the toxicity testing.

The optimal measurement frequency allows the sensors to obtain the largest difference in measured impedance between a sample with and without cells [19]. In this study, the impedance of cell monolayer was measured with different frequencies from 500 Hz to 64 kHz. The optimal measurement frequency was optimized to be 8000 Hz in experimental measurements.

5.5 Toxicity testing

The ECIS sensors need to be prepared before the toxicity testing. ECIS sensors were cleaned by oxygen plasma to provide a sterilized surface for cell seeding. Then phosphate-buffered saline (PBS, GIBCO, Grand Island, NY) was used to clean the sensor surface again. Before cell seeding, 30 µg/ml fibronectin (GIBCO, Grand Island, NY) was coated on the surface of the sensors to improve cell attachment. BAECs were seeded onto each sensor with a seeding density of 125,000 cells/cm². The cell morphology was checked under microscope. The selected toxicants were introduced to each well to perform toxicity testing after monolayer formation. **Figure 12** shows normalized impedance response after introducing 0.1 and 0.2 mM aldicarb and the cell morphology after introducing 0.2 mM aldicarb. Some of the cells detached from the substrate. The normalized impedance decreases to 0.84 and

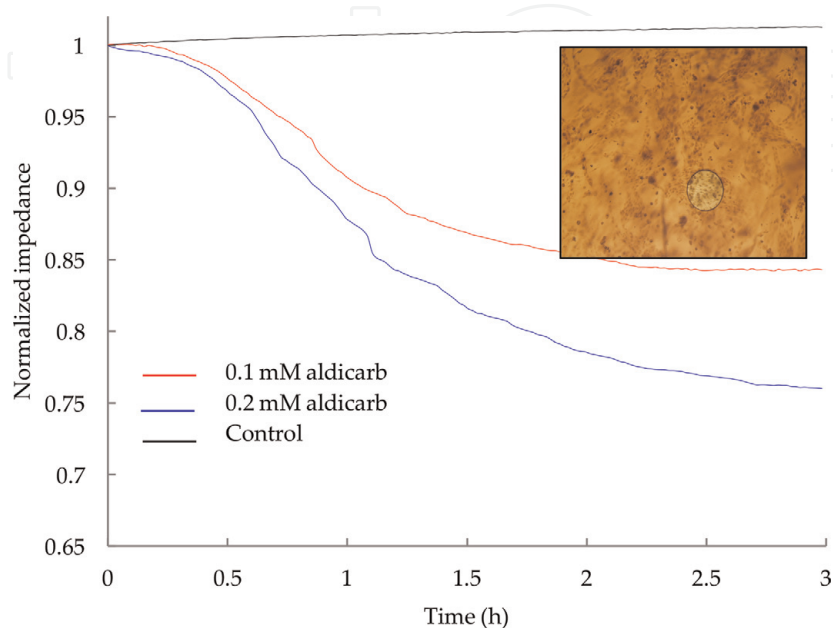


Figure 12.
The normalized impedance of BAEC exposed to aldicarb.

0.76 times its original impedance value within 3 hours when treated with 0.1 and 0.2 mM aldicarb, respectively. The cell morphology changed and even detached from the sensors. **Figure 13** shows the normalized impedance response after introducing 0.1 and 0.2 mM phenol as toxicant. The BAEC detached from substrate after introducing 0.2 mM phenol. The decreasing impedance curves indicate the toxic effect on BAECs. The normalized impedance values rapidly decreased to 0.80 and 0.74 times its original impedance value within 2 hours when treated with 0.1 and 0.2 mM phenol, respectively. The image shows the cells obviously detached from the sensor. **Figure 14** shows the normalized impedance response after introducing 2 and 5 mM ammonia as toxicant. Those lines shows that the normalized impedance values rapidly decreased to 0.78 and 0.68 times its original impedance value within 1 hour when treated with 2 and 5 mM ammonia, respectively. The image shows the cell morphology after 1 hour after introducing ammonia. The cells morphology changed and very easily detached from the sensor substrate. **Figure 15** shows the

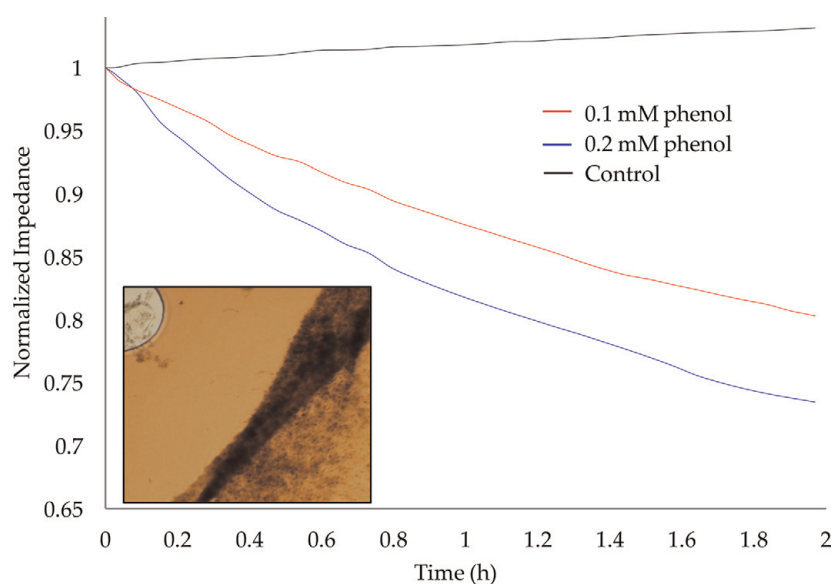


Figure 13.
The normalized impedance of BAEC exposed to phenol.

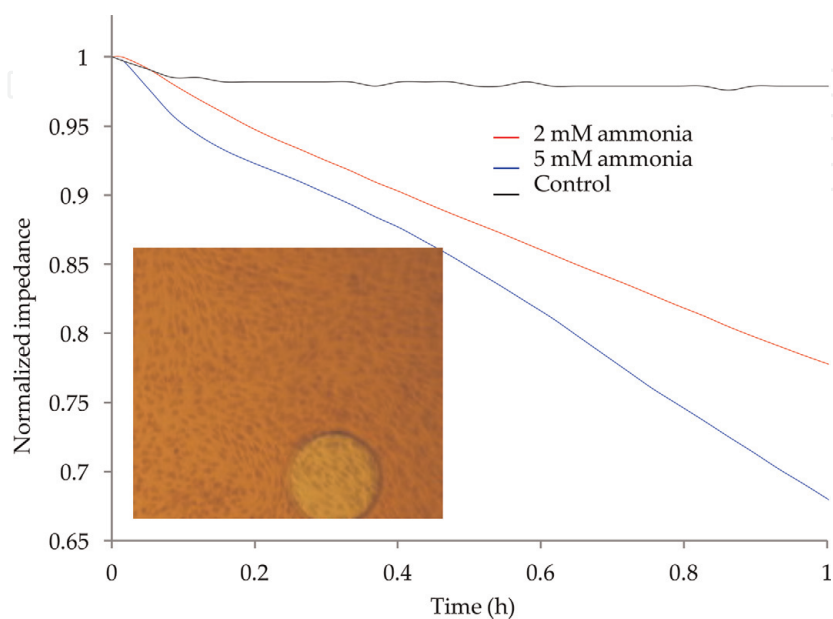


Figure 14.
The normalized impedance of BAEC exposed to 2 mM and 5 mM ammonia, and the image shows the BAEC morphology after exposure to 5 mM of ammonia.

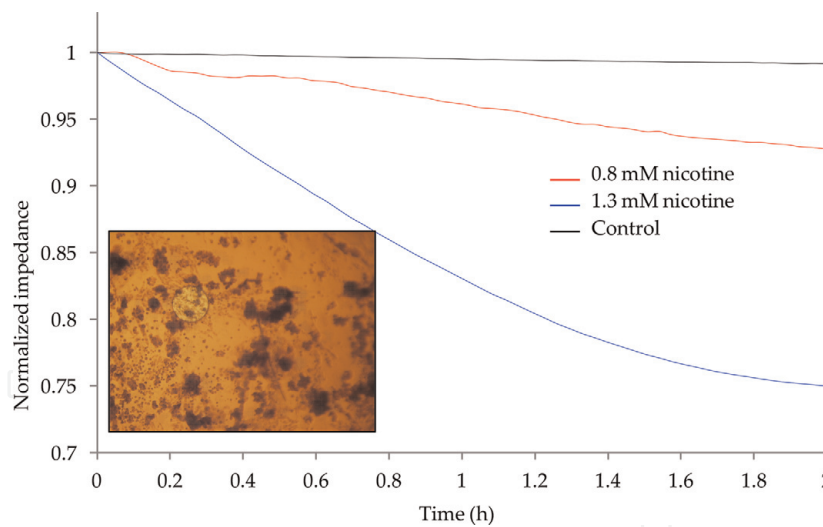


Figure 15.

The normalized impedance of BAEC exposed to 0.8 mM and 1.3 mM nicotine. The image shows the cell morphology after exposure to 1.3 mM nicotine.

normalized impedance of BAEC after exposing to 0.8 and 1.3 mM nicotine as toxicant. The normalized impedance rapidly decreased to 0.92 and 0.75 times its original value within 2 hours when treated with 1.3 and 0.8 mM nicotine, respectively. The image shows the BAEC morphology after exposed to 1.3 mM nicotine. Most of the cell detached from the sensor due to the toxic effect of nicotine.

The cell morphology and decreasing impedance curves indicate the toxic effect and the effectiveness of ECIS sensing on environmental monitoring within short period of time. Different concentrations of toxicants are qualified according to the gradients of normalized impedance. ECIS sensing technique is able to perform environmental monitoring effectively and efficiently compared with other approaches.

6. Conclusions

In this study, the biosensors based on ECIS sensing technique were used to monitor and measure the environmental toxicants, including the phenol, ammonia, nicotine, and aldicarb. A model, validated by experimental results, was created to analyze the electric potential distribution of ECIS sensing and guide the designing, especially the sensing area of sensor electrodes. The detection sensitivity of ECIS sensors was optimized. The experimental results show that ECIS sensors are capable to detect and qualify the environmental toxicants rapidly. The concentration of toxicants can be indicated from the gradients of normalized cell impedance.

Acknowledgements

We appreciate Dr. Ioana Voiculescu's and Andres Rivera's support in this study.

IntechOpen

Author details

Xudong Zhang^{1*}, William Wang² and Sunghoon Jang³

1 City University of New York, New York, USA

2 Stanford University, Stanford, USA

3 New York City College of Technology of City University of New York, USA

*Address all correspondence to: xzhang19@citymail.cuny.edu

IntechOpen

© 2018 The Author(s). Licensee IntechOpen. This chapter is distributed under the terms of the Creative Commons Attribution License (<http://creativecommons.org/licenses/by/3.0>), which permits unrestricted use, distribution, and reproduction in any medium, provided the original work is properly cited. 

References

- [1] Giaever I, Keese C. Monitoring fibroblast behavior in tissue culture with an applied electric field. *Proceedings of the National Academy of Sciences*. 1984; **81**:3761-3764
- [2] Giaever I, Keese CR. Use of electric fields to monitor the dynamical aspect of cell behavior in tissue culture. *IEEE Transactions on Biomedical Engineering*. 1986; **33**:242-247
- [3] Mitra P, Keese CR, Giaever I. Electric measurements can be used to monitor the attachment and spreading of cells in tissue culture. *BioTechniques*. 1991; **11**: 504-510
- [4] Tiruppathi C, Malik AB, Del Vecchio PJ, Keese CR, Giaever I. Electrical method for detection of endothelial cell shape change in real time: Assessment of endothelial barrier function. *Proceedings of the National Academy of Sciences*. 1992; **89**:7919-7923
- [5] Pei Z, Keese CR, Giaever I, Kurzawa H, Wilson DE. Effect of the pSV2-neo plasmid on NIH 3T3 cell motion detected electrically. *Experimental Cell Research*. 1994; **212**:225-229
- [6] Keese CR, Giaever I. A biosensor that monitors cell morphology with electrical fields. *IEEE Engineering in Medicine and Biology Magazine*. 1994; **13**:402-408
- [7] Voiculescu I, Zhang X, Cell-on-chip stretchable platform for mammalian cells with integrated impedance spectroscopy technique. In: *Google Patents*; 2017
- [8] Zhang X, Nordin AN, Li F, Voiculescu I. Stretchable lab-on-chip device with impedance spectroscopy capability for mammalian cell studies. In: *Proceedings of the ASME 2016 International Mechanical Engineering Congress and Exposition; American Society of Mechanical Engineers*; 2016. pp V010T13A005-V010T13A005
- [9] Zhang X, Wang W, Li F, Voiculescu I. Stretchable impedance sensor for mammalian cell proliferation measurements. *Lab on a Chip*. 2017; **17**: 2054-2066
- [10] Zhang X. Stretchable impedance spectroscopy sensor for mammalian cell studies [thesis]. The City College of New York; 2016
- [11] Zhang X, Li F, Lee K, Voiculescu I. Lab-on-chip stretchable impedance spectroscopy device for mammalian cells studies. In: *Proceedings of 19th International Conference on the Solid-State Sensors, Actuators and Microsystems (TRANSDUCERS)*; IEEE; 2017. pp. 1563-1566
- [12] Zhang X, Petrissans R, Li F, Voiculescu I. Stretchable impedance spectroscopy sensor for mammalian cells impedance measurements. In: *Proceedings of the ASME 2014 International Mechanical Engineering Congress and Exposition; American Society of Mechanical Engineers*; 2014. pp. V010T13A005-V010T13A005
- [13] Voiculescu I, Li F, Liu F, Zhang X, Cancel LM, Tarbell JM, et al. Study of long-term viability of endothelial cells for lab-on-a-chip devices. *Sensors and Actuators B: Chemical*. 2013; **182**: 696-705
- [14] Ayliffe HE, Frazier AB, Rabbitt RD. Electric impedance spectroscopy using microchannels with integrated metal electrodes. *Journal of Microelectromechanical Systems*. 1999; **8**:50-57
- [15] Han A, Moss E, Frazier AB. Whole cell electrical impedance spectroscopy for studying ion channel activity. In: *Proceedings of the 13th International*

Conference on Solid-State Sensors, Actuators and Microsystems, 2005. Digest of Technical Papers. TRANSDUCERS'05; IEEE; 2005. pp. 1704-1707

[16] Han A, Yang L, Frazier AB. Quantification of the heterogeneity in breast cancer cell lines using whole-cell impedance spectroscopy. *Clinical Cancer Research*. 2007;**13**:139-143

[17] Solly K, Wang X, Xu X, Strulovici B, Zheng W. Application of real-time cell electronic sensing (RT-CES) technology to cell-based assays. *Assay and Drug Development Technologies*. 2004;**2**: 363-372

[18] Zhang X, Li F, Nordin AN, Tarbell J, Voiculescu I. Toxicity studies using mammalian cells and impedance spectroscopy method. *Sensing and Bio-Sensing Research*. 2015;**3**:112-121

[19] Zhang X, Wang W, Nordin AN, Li F, Jang S, Voiculescu I. The influence of the electrode dimension on the detection sensitivity of electric cell-substrate impedance sensing (ECIS) and its mathematical modeling. *Sensors and Actuators B: Chemical*. 2017;**247**: 780-790

[20] Wang L, Wang H, Mitchelson K, Yu Z, Cheng J. Analysis of the sensitivity and frequency characteristics of coplanar electrical cell-substrate impedance sensors. *Biosensors and Bioelectronics*. 2008;**24**:14-21

[21] Öz S, Maercker C, Breiling A. Embryonic carcinoma cells show specific dielectric resistance profiles during induced differentiation. *PLoS One*. 2013;**8**:e59895

[22] Gentet LJ, Stuart GJ, Clements JD. Direct measurement of specific membrane capacitance in neurons. *Biophysical Journal*. 2000;**79**:314-320

[23] Lo C-M, Keese CR, Giaever I. Impedance analysis of MDCK cells

measured by electric cell-substrate impedance sensing. *Biophysical Journal*. 1995;**69**:2800

[24] Asphahani F, Zhang M. Cellular impedance biosensors for drug screening and toxin detection. *The Analyst*. 2007;**132**:835-841

[25] Spira ME, Hai A. Multi-electrode array technologies for neuroscience and cardiology. *Nature Nanotechnology*. 2013;**8**:83-94

[26] Li H, Zou Q, Zou L, Wang Q, Su K, Hu N, et al. Detection of cardiovascular drugs and marine toxins using a multifunctional cell-based impedance biosensor system. *Analytical Methods*. 2015;**7**:7715-7723

[27] Wang J, Wu C, Hu N, Zhou J, Du L, Wang P. Microfabricated electrochemical cell-based biosensors for analysis of living cells in vitro. *Biosensors*. 2012;**2**:127-170

[28] Anderson SE, Bau HH. Electrical detection of cellular penetration during microinjection with carbon nanopipettes. *Nanotechnology*. 2014;**25**: 245102

[29] Giaever I, Keese CR. Micromotion of mammalian cells measured electrically. *Proceedings of the National Academy of Sciences*. 1991;**88**: 7896-7900

[30] Chen J, Zheng Y, Tan Q, Shojaei-Baghini E, Zhang YL, Li J, et al. Classification of cell types using a microfluidic device for mechanical and electrical measurement on single cells. *Lab on a Chip*. 2011;**11**:3174-3181

[31] Chen J, Zheng Y, Tan Q, Zhang YL, Li J, Geddie WR, et al. A microfluidic device for simultaneous electrical and mechanical measurements on single cells. *Biomicrofluidics*. 2011;**5**:014113

[32] Park S, Zhang Y, Wang T-H, Yang S. Continuous dielectrophoretic

- bacterial separation and concentration from physiological media of high conductivity. *Lab on a Chip*. 2011;**11**: 2893-2900
- [33] McNutt NS, Weinstein RS. The ultrastructure of the nexus: A correlated thin-section and freeze-cleave study. *The Journal of Cell Biology*. 1970;**47**: 666-688
- [34] Bohnert J. Effects of Time-Varying Magnetic Fields in the Frequency Range 1 kHz to 100 kHz upon the Human Body: Numerical Studies and Stimulation Experiment. Karlsruhe: KIT Scientific Publishing; 2014
- [35] Iwanaga Y. Cell-substrate distance measurement in correlation with distribution of adhesion molecules by fluorescence microscopy [thesis]. Technische Universität München; 2000
- [36] Lang Q, Wu Y, Ren Y, Tao Y, Lei L, Jiang H. AC electrothermal circulatory pumping chip for cell culture. *ACS Applied Materials & Interfaces*. 2015;**7**: 26792-26801
- [37] Randles JEB. Kinetics of rapid electrode reactions. *Discussions of the Faraday Society*. 1947;**1**:11-19
- [38] Schwan H. Electrode polarization impedance and measurements in biological materials. *Annals of the New York Academy of Sciences*. 1968;**148**: 191-209
- [39] Warburg E. Ueber das Verhalten sogenannter unpolarisierbarer Elektroden gegen Wechselstrom. *Ann. Phys.* 1899;**303**:493-499
- [40] Lvovich VF. Impedance Spectroscopy: Applications to Electrochemical and Dielectric Phenomena. Hoboken: John Wiley & Sons; 2012
- [41] Nguyen TA, Yin T-I, Reyes D, Urban GA. Microfluidic chip with integrated electrical cell-impedance sensing for monitoring single cancer cell migration in three-dimensional matrixes. *Analytical Chemistry*. 2013;**85**: 11068-11076
- [42] Franks W, Schenker I, Schmutz P, Hierlemann A. Impedance characterization and modeling of electrodes for biomedical applications. *IEEE Transactions on Biomedical Engineering*. 2005;**52**:1295-1302
- [43] Henisch HK. Rectifying Semiconductor Contacts. Oxford: Clarendon Press; 1957
- [44] Kovacs GT. Introduction to the Theory, Design, and Modeling of Thin-Film Microelectrodes for Neural Interfaces. San Diego: Academic Press; 1994. pp. 121-165
- [45] Schroder DK. Semiconductor Material and Device Characterization. Hoboken: John Wiley & Sons; 2006
- [46] Joye N, Schmid A, Leblebici Y. An electrical model of the cell-electrode interface for high-density microelectrode arrays. In: Proceedings of the 30th Annual International Conference of the IEEE Engineering in Medicine and Biology Society; IEEE; 2008. pp. 559-562
- [47] Alberto Yf, Alberto O. Cell Biometrics Based on Bio-Impedance Measurements. In: Chetty G, editors. Advanced biometric technologies. London: InTech; 2011 p. 343-366. DOI: 10.5772/21742
- [48] Xue P, Bao J, Chuah YJ, Menon NV, Zhang Y, Kang Y. Protein covalently conjugated SU-8 surface for the enhancement of mesenchymal stem cell adhesion and proliferation. *Langmuir*. 2014;**30**:3110-3117